Applied Surface Science 284 (2013) 372–378

Contents lists available at ScienceDirect

Applied Surface Science

journal homepage: www.elsevier.com/locate/apsusc

A simple method for fabrication of high-aspect-ratio all-silicon grooves

Yuncan Ma, An Pan, Jinhai Si *, Tao Chen, Feng Chen, Xun Hou

Key Laboratory for Physical Electronics and Devices of the Ministry of Education & Shaanxi Key Laboratory of Information Photonic Technique, School of Electronics & Information Engineering, Xi'an Jiaotong University, No. 28, Xianning West Road, Xi'an 710049, China

ARTICLE INFO

Article history:
Received 20 May 2013
Accepted 20 July 2013
Available online 29 July 2013

Keywords:
All-silicon groove
Refractive index change
Chemical selective etching
Femtosecond laser

ABSTRACT

A simple method using 800-nm femtosecond laser irradiation and chemical selective etching has been proposed for fabrication of high-aspect-ratio all-silicon grooves. Grooves with the maximum aspect ratio of 44 were produced. A scanning electronic microscopy equipped with an energy dispersive X-ray spectroscopy was employed to characterize the morphology and chemical composition of the grooves respectively. The formation mechanism of the grooves was attributed to the chemical reaction of the laser induced refractive index change microstructures and hydrofluoric acid solution. The dependences of the aspect ratio of the grooves on the laser irradiation parameters, such as: the numerical aperture of the microscope objective lens, the laser average power and the laser scanning velocity, are discussed.

© 2013 Elsevier B.V. All rights reserved.

1. Introduction

High-aspect-ratio (HAR) silicon grooves have inspired increasing research interests due to their potential applications in microelectronics, optoelectronics, microchemical systems, microelectromechanical systems (MEMS), microbiology and so on. Accordingly, researchers have successfully fabricated different kinds of silicon-based devices with HAR grooves, such as isolation grooves and through-silicon-via (TSV) structures in semiconductor devices [1–4], one/two/three dimension photonic crystals (1/2/3D PhCs) [5–7], surface plasmon polariton assisted THz transmission devices [8], microchemical reactors [9], microsensors [10] and so on.

Generally, the traditional technologies for fabrication of silicon grooves could be divided into two categories based on the process methods, i.e., dry etching and wet etching. The former mainly refers to reactive ion etching (RIE). There have been plenty of literatures on the silicon grooves produced via RIE. Some examples of these are: by using low temperature RIE technology, Tachi et al. produced silicon grooves, which have the aspect ratio (AR) of about 3, the depth of 3 μm and the width of 1 μm [11], with sulphur hexafluoride (SF_6) gas plasma; while using deep reactive ion etching (DRIE) technology, St-Gelais et al. fabricated an all-silicon Fabry-Pérot refractometer, with the AR of the grooves was about 30, the depth of 80 μm and the width of 2.6 μm [12]. In order to obtain smoother sidewalls of the grooves and higher etching selectivity of silicon to the mask or photoresist (PR), near-room temperature high density plasma (HDP) etching, in which the inductively coupled plasma (ICP) and reactive ion etching (RIE) plasma resources were utilized, was explored [13]. The later mainly refers to alkaline solutions based wet anisotropic etching, in which the potassium hydroxide (KOH) solution was commonly employed [14–17], was also a popular approach to fabricate HAR silicon grooves. Some examples include: by using KOH solution based wet etching, Tolmachev et al. fabricated 1D PhCs in n-type (1 1 0) silicon wafers, with the AR of the grooves of 16, the depth of about 54 μm and the width of 3.4 μm [15]; Bengtsson et al. fabricated a silicon-based micro-enzyme reactor (μMER), with the AR of the silicon grooves of 4, the depth of 200 μm and the width of 50 μm [17]. However, since the KOH solution based wet anisotropic etching is orientation-dependent, the etching rate on the plane of (1 1 1) is dramatically slower than that on (1 0 0) or (1 1 0). This fundamentally limits the applications of wet etching technology to silicon wafers with other crystal orientations. With respect to the two typical silicon etching technologies introduced above, a significant drawback is the need for mask materials. The deposition, patterning, and subsequent removal of such masks add considerable complexity to the silicon groove fabrication process. Meanwhile, the controllability of the AR of the grooves and the selectivity of silicon to masks are not ideal. In recent years, the combination of dry and wet etching was also introduced to overcome the shortcomings of these two technologies; however, this still could not easily simplify the technological progress or improve the quality of the grooves.

More recently, laser direct etching has proved to be an effective and feasible approach to produce silicon grooves. Several investigations have been conducted on the fabrication of silicon grooves

* Corresponding author.
E-mail address: jinhaisi@mail.xjtu.edu.cn (J. Si).

0169-4332/$ – see front matter © 2013 Elsevier B.V. All rights reserved.
http://dx.doi.org/10.1016/j.apsusc.2013.07.107

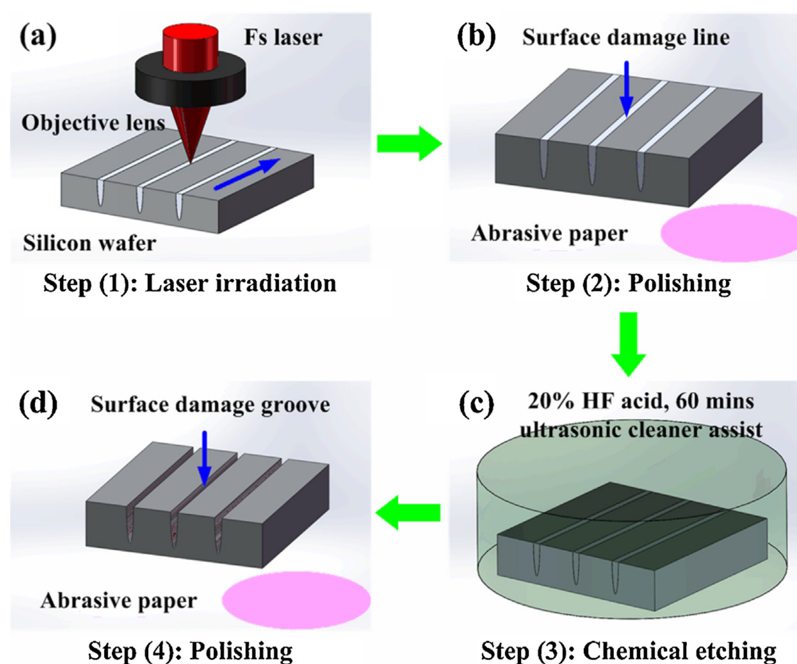

Fig. 1. Technological process for the fabrication of the silicon-based grooves: (a) laser irradiation; (b) polishing: RIC microstructures; (c) chemical selective etching; (d) polishing: grooves. The blue arrow in (a) illustrates the scanning direction of the laser beam. (For interpretation of the references to color in figure legend, the reader is referred to the web version of the article.)

by continuous wavelength (CW) laser [18–20] or femtosecond laser [21], and the HAR was achieved by the means of multiple passes of the incident laser beam on the silicon wafers [21] or by using high-repetition-rate laser [22]. However, since these experiments were performed in ambient air, the chemical composition of the induced grooves would not be pure silicon anymore. This means that foreign species, especially oxygen (O), would contaminate the photoinduced grooves. This is not significantly tolerable in the integration of silicon-based chips with other devices. Therefore, exploring fabrication methods for the all-silicon grooves with better quality is needed.

In this paper, a simple method for the fabrication of HAR all-silicon grooves via the combination of the 800-nm femtosecond laser irradiation and chemical selective etching with hydrofluoric (HF) acid solution was proposed. With the 800-nm femtosecond laser irradiation, refractive index change (RIC) microstructures were induced at the irradiated zones. Via the selective etching with HF acid solution, the RIC microstructures sacrificed and then the grooves formed. In our experiments, a scanning electronic microscopy (SEM) equipped with an energy dispersive X-ray spectroscopy (EDS) was employed to characterize the morphology and chemical compositions of the RIC microstructures and the silicon grooves, respectively. Results show that the maximum AR of the RIC microstructures and grooves was 44, with the depth of 286 μm and the width of 6.5 μm. Meanwhile, the main chemical composition of the grooves was silicon. Furthermore, the formation mechanism of the silicon grooves and the dependences of the AR of the grooves on the laser irradiation parameters are discussed.

2. Experimental details

2.1. Technological process

The technological process for the fabrication of the silicon-based grooves is divided into four steps chronologically, as illustrated in Fig. 1.

2.1.1. Laser irradiation

The p-type (1 0 0) silicon wafers, with a thickness of 500 μm and a resistivity of 1–5 Ωm, were mounted horizontally on a computer controlled three dimensional (3D) translation stage (ProScan II^{TM}). Prior to the laser irradiation, the silicon wafers were rinsed successively in an ultrasonic cleaner with acetone, ethanol, and de-ionized water for 20 min, respectively. An amplified Ti: sapphire femtosecond laser system (Coherent Inc., U.S.A.) was employed to provide laser pulses with 50-fs pulse duration, 800-nm wavelength, and 1-kHz repetition rate. The intensity distribution of the incident laser was Gaussian-type. The average power of the incident laser pulses could be continuously varied by rotating a variable neutral density filter (NDF), and the access of the laser beam was controlled via a mechanical shutter connected to the computer. The horizontally polarized femtosecond laser beam was focused perpendicularly onto the silicon wafers by a microscope objective lens (Nikon), and the scanning direction was parallel to the polarization direction of the incident laser. The distance between two adjacent scanning lines (Δd), which could be varied via the software equipped with the 3D translation stage, was set at 80 μm. A charge coupled device (CCD) camera (Nikon) connected to the computer was employed to monitor the irradiation process on line. Meanwhile, the irradiation was performed in ambient air, with the temperature and the humidity of 22 $^\circ$C and 40%, respectively.

2.1.2. Polishing-RIC microstructures

Since silicon was opaque material, the observation of the microstructures fabricated in the interior of silicon was not as convenient as those in transparent materials; therefore, the irradiated silicon wafers were polished with water proof abrasive papers to a random position to observe the photoinduced RIC microstructures from the cross section.

2.1.3. Chemical selective etching

After polishing, the silicon wafers were etched with 20 wt% HF acid solution for 60 min to remove the RIC microstructures in an ultrasonic cleaner. There were two advantages for the chemical

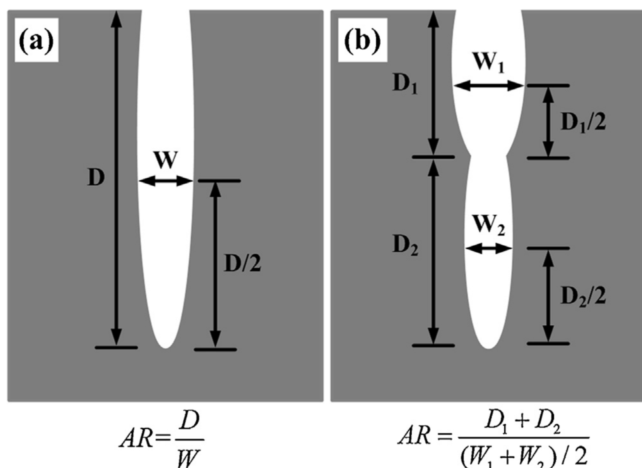

Fig. 2. Diagrammatic sketch for the definition of the aspect ratio (AR) of the grooves: (a) the cross-sectional shape is single ellipse and (b) the cross-sectional shape is multiple ellipses.

etching performed in an ultrasonic cleaner. Firstly, in the ultrasonic environment, the by-products of the chemical etching could quickly escape from the silicon surface to the ambient solution, which would weaken the loading effect in the chemical etching process, this was beneficial to the chemical reaction. Secondly, the temperature of the ambient water rose from 20 °C to 40 °C in ultrasonic shocking process; this would accelerate the progress of the chemical etching.

2.1.4. Polishing-grooves

For the purpose of examining the continuity of the chemical selective etching induced grooves, the etched silicon wafers were carefully polished to random positions along the laser scanning direction. The grooves could be observed at any position from the cross section, and the variation of the depth and width was little. This suggests that the continuity of the silicon grooves was well.

2.2. Characterization of the grooves and RIC microstructures

The morphology and chemical composition of the photoinduced RIC microstructures and the chemical selective etching induced grooves were characterized by a scanning electronic microscopy (SEM, FEI Quanta 250 FEG Serials) equipped with an energy dispersive X-ray spectroscopy (EDS, TEAM^{TM} Serials), respectively.

2.3. Definition of AR of the silicon grooves

The AR of the grooves was defined as following: when the cross-sectional shape of the groove is single ellipse, as shown in Fig. 2(a), the AR of the groove is AR = D/W, D is the depth of the groove, and W is the width of the groove at the half depth; when the cross-sectional shape of the groove is multiple ellipses (or approximate to single taper), as shown in Fig. 2(b), the AR of the groove is AR = $(D_1 + D_2)/((W_1 + W_2)/2)$, D_1, D_2 are the depths of single ellipse, and W_1, W_2 are the widths at half depth accordingly.

3. Results and discussion

3.1. Formation mechanism of silicon grooves

Fig. 3 illustrates the morphology and chemical composition of both the photoinduced RIC microstructures and the chemical etching induced silicon grooves, respectively. The laser irradiation parameters are: P = 30.0 mW, υ = 2 μm/s, NA = 0.30 (10×), Δd = 80 μm; the chemical etching conditions are: 20 wt% HF acid solution, 60 min, with ultrasonic cleaner assisting. With the 800-nm femtosecond laser irradiation, RIC microstructures were induced at the irradiated zones along the longitudinal direction of the femtosecond laser transmission, which are shown in Fig. 3(a) as the gray lines. The depth and the half width of the RIC microstructures were about 270 μm and 7.6 μm, respectively. As far as we know, there have been no reports on the 800-nm femtosecond laser induced RIC microstructures in the interior of silicon, and the formation mechanism of the RIC microstructures is still an open question. Fig. 3(b) illustrates the chemical compositions of the RIC microstructures obtained from the EDS analysis. It can be seen from Fig. 3(b) that the foreign O species was incorporated into the interior of the silicon substrates, and its content decreased with the increase of the RIC depth. The incorporation mechanism of the foreign O species into the interior of silicon could be attributed to the femtosecond laser induced trapping effect of the dangling bonds [23,24]. When the silicon wafers were irradiated by the femtosecond laser pulses, the original regular tetrahedron crystal structures of silicon material were disordered; therefore, dangling bonds, which could trap the O atoms from ambient air into the interior of silicon material, appeared in the silicon crystal lattices. Meanwhile, since the density of the femtosecond laser induced dangling bonds decreased with the decrease of the laser intensity, the number of the dangling bonds decreased as the laser transmits along the longitudinal direction. This resulted in the decrease of the atomic percentage of the incorporated O species with the increase of the RIC depth, and the O species existed in the RIC microstructures in the form of silicon dioxide (SiO_2).

After the femtosecond laser irradiation, the silicon wafers with RIC microstructures were ultrasonically immersed in 20 wt% HF acid solution for 60 min, then the RIC microstructures were removed due to the chemical reaction of HF acid solution with SiO_2, and the related chemical reactive formulas could be expressed as [24–26]:

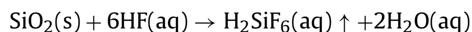

$$SiO_2(s) + 6HF(aq) \rightarrow H_2SiF_6(aq)\uparrow + 2H_2O(aq)$$

This means that the RIC microstructures sacrifice after the HF acid solution etching; and this leads to the formation of the silicon grooves. This method for the silicon grooves could be called combination of femtosecond laser irradiation and chemical selective etching.

In this method, the HF acid solution merely reacts with SiO_2 in the RIC microstructures, but the surrounding zones remain unchanged, which indicates the selectivity of the chemical etching is high. After the HF acid solution etching, the wafers were rinsed in the ultrasonic cleaner with ethanol and de-ionized water for 20 min to eliminate the remained reactant HF acid and the by-product fluosilicic acid (H_2SiF_6), respectively. According to the SEM morphology and chemical composition of the grooves illustrated in Fig. 3(c)–(f), the sidewalls of the silicon grooves, with few micro grass left on, were smoother than those fabricated by laser direct etching only [18–22,27]. Meanwhile, the atomic percentage of O species in surrounding of the grooves marked in these images were all in the region of the measurement deviation of the EDS analysis, which could be ignored; therefore, the main chemical composition of the grooves was silicon, and the grooves fabricated here could be called all-silicon grooves.

To the best of our knowledge, there have been no reports on the all-silicon grooves fabrication via this method. Comparing this method to the dry or wet etching technologies for silicon grooves [11–14,28–32], the main advantages of this method could be summarized as following: Firstly, since the femtosecond laser irradiation is a maskless process, no mask or photoresist (PR) is needed; therefore, the cost for the fabrication of the silicon grooves

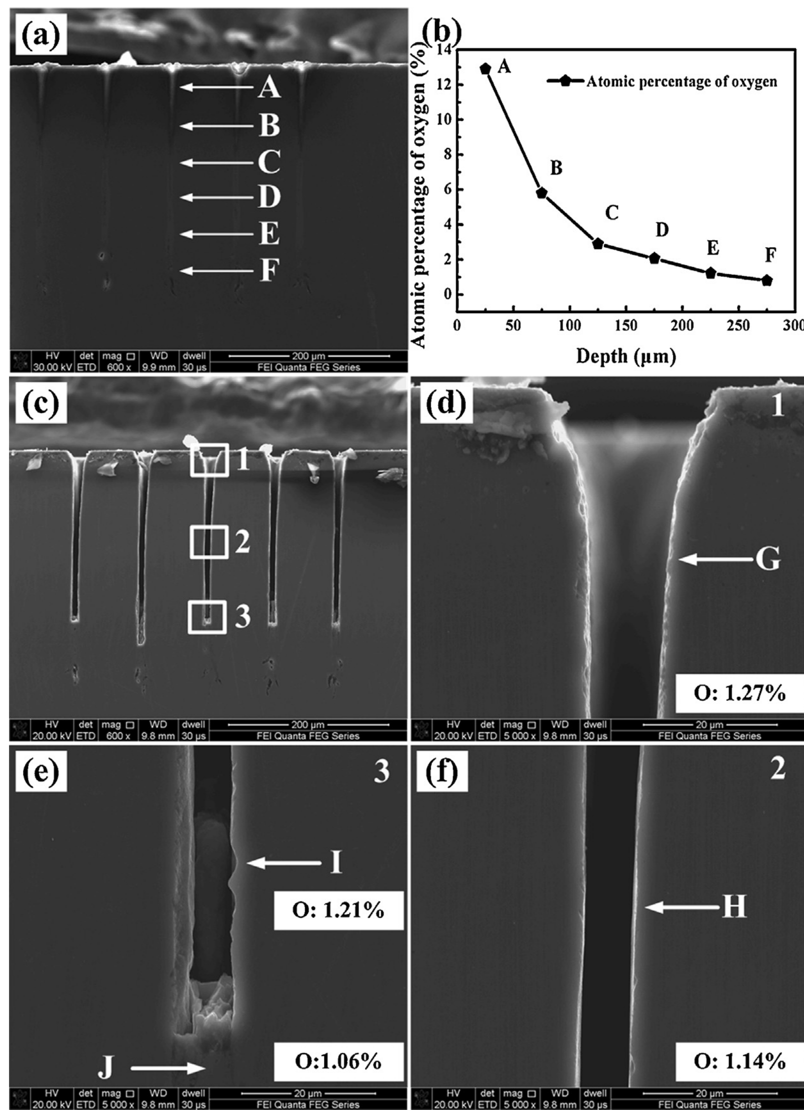

Fig. 3. SEM images of the RIC microstructures and the chemical selective etching induced grooves (view from the cross section). (a) The laser induced RIC microstructures; (b) atomic percentage of O species along the longitudinal direction of the RIC microstructures, the measured points are marked in (a); (c) the chemical selective etching induced grooves; (d) detailed morphology of the groove at the entrance surface; (e) detailed morphology of the groove at the tail; (f) detailed morphology of the grooves at the half depth. The atomic percentage of the oxygen (O) species is given in (d)–(f). (For interpretation of the references to color in figure legend, the reader is referred to the web version of the article.)

is much lower. Secondly, in current silicon etching technologies for HAR grooves, the technological process, including mask or PR deposition, silicon etching and mask or PR removing, is too complicated; however, the method for silicon grooves proposed here dramatically simplifies the technological process, which makes the fabrication of the silicon grooves achievable in any laser machining research laboratory. Thirdly, the etching rates of this method are much higher than those of the traditional technologies. Finally, since the formation mechanism of the silicon grooves is attributed to the chemical reaction of SiO_2 and HF acid solution, this method could be applied to the etching of other single crystal silicon, regardless of the crystallographic orientations or crystal types, such as n/p-Si (1 0 0), n/p-Si (1 1 1), n/p-Si (1 1 0) and so on. Being able to etch silicon wafers along any crystal orientation is likely to open up a new dimension in silicon electronics and potential applications, and this suggests that the flexibility of this method is high. Meanwhile, comparing this method to the laser direct etching for silicon grooves [18–22,27], the foreign O species is effectively eliminated by the HF acid solution etching. This is of great importance to the integration of the silicon chips with these grooves to other microfluidic networks or semiconductor devices. Because of its low cost, high selectivity, high etching rate, high flexibility, and high potential impact-on, we predict that this would be a promising method for the fabrication of silicon-based advanced functional materials. The all-silicon grooves produced by this method could find some potential applications in the super hydrophobic microstructures [33,34], optofluidic microsystems (OFMs) for label-free biological or chemical analysis [35,36], silicon molds [37,38] in the field of MEMS, and so on. What's more, due to the good quality of the induced grooves, the method proposed here could be developed to become an alternative and practical strategy for thin silicon wafers cutting. This could solve the problems, such as fragility of the thin wafers and irregularity of the cutting edge, which exist in the traditional methods for the thin wafer cutting via wafer knife cutting and laser cutting only.

According to the formation mechanism of the silicon grooves discussed above, the AR of the silicon grooves is dependent on the femtosecond laser irradiation parameters and the chemical etching conditions. In the following sections, we mainly discuss the dependence of AR on the femtosecond laser irradiation parameters.

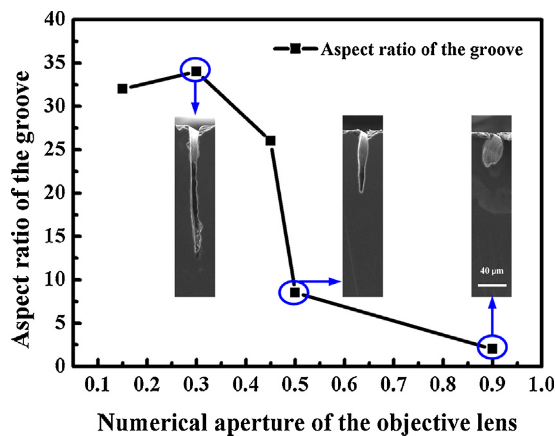

Fig. 4. Dependence curve of AR on the numerical aperture of the objective lens (NA). The scale in the inset is 40 μm. (For interpretation of the references to color in figure legend, the reader is referred to the web version of the article.)

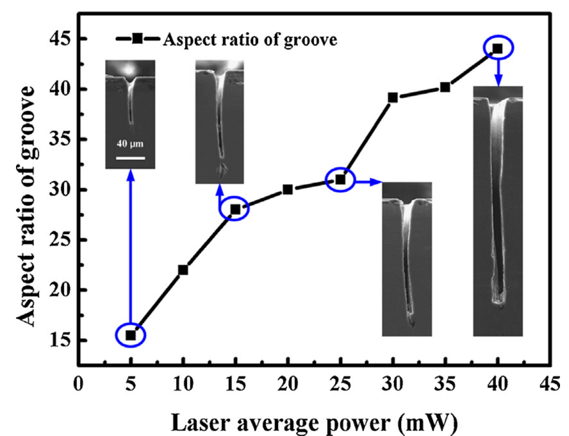

Fig. 5. Dependence curve of AR on the laser average power (*P*). The scale in the inset is 40 μm. (For interpretation of the references to color in figure legend, the reader is referred to the web version of the article.)

3.2. Dependence of AR on the laser irradiation parameters

3.2.1. AR versus NA

Fig. 4 illustrates the dependence curve of AR of the silicon grooves on the NA of the microscope objective lens, and the insets show the morphology of the silicon grooves accordingly. The laser irradiation parameters are: $P = 30.0$ mW, $\upsilon = 5$ μm/s, $\Delta d = 80$ μm. The chemical etching conditions are: 20 wt% HF acid solution, 60 min, with ultrasonic cleaner assisting. It can be seen from the curve in Fig. 4 that the AR decreases with the increase of NA. Some examples are as following: when the value of NA is 0.30 (10×), the AR is 34, with the depth of 208 μm and the width of 6.2 μm; when the value of NA is 0.50 (50×), the AR is 8.5, with the depth of 100.4 μm and the average width of 12.4 μm; when the value of NA increases to 0.90 (90×), the AR is 2, with the depth of 61.2 μm and the width of 30.6 μm. It can also be seen from the insets in Fig. 4 that the cross-sectional shape of the groove changes from multiple ellipses (approximate to single taper) to single ellipse, and the entrance width of the silicon groove decreases with the increase of NA.

As we know, the numerical aperture (NA), which characterizes the focus capacity of the lens to the incident laser beam, is a key parameter of the microscope objective lens. The larger the NA of the objective lens, the smaller the laser spot sizes at the focal plane and the shallower the focal depth. Therefore, under the same laser average power and the same scanning velocity, the entrance width and depth of the RIC microstructures decreases with the increase of NA. Meanwhile, there exists the competition between the self-focusing due to the nonlinear Kerr effect and the self-defocusing results from the thermal accumulation in femtosecond laser irradiation [39]. When the laser beam is loosely focused (NA < 0.50) onto the silicon wafers, the self-defocusing is dominant. As a result, the cross-sectional shapes of the photoinduced RIC microstructures are multiple slim ellipses (approximate to single taper); when the laser beam is tightly focused (NA > 0.50) onto the silicon wafers, the self-focusing is remarkable. This makes the cross-sectional shapes of the RIC microstructures are single fat ellipses. Since the decreasing extent of the depth is much higher than that of the width, the AR of the silicon grooves decreases with the increase of NA. Meanwhile, under the same laser average power and the same laser scanning velocity, the larger the NA of the objective lens, the higher the intensity of the laser irradiated on the silicon substrates. This means more laser induced dangling bonds would appear at the irradiated zones, therefore, more foreign O species could be incorporated into the interior of silicon, which makes the RIC microstructures be more effectively eliminated via the HF acid solution etching. Based on the analysis of the dependency of AR and cross-sectional shape on NA, the microscope objective lens with the NA of 0.30 (10×) was employed to fabricate RIC microstructures with single tapered cross-sectional shape for silicon grooves.

3.2.2. AR versus P

Fig. 5 illustrates the dependence curve of the AR of the grooves on the laser average power, and the insets show the morphology of the grooves accordingly. The laser irradiation parameters are: NA = 0.30 (10×), $\upsilon = 5$ μm/s, $\Delta d = 80$ μm. The chemical etching conditions are: 20 wt% HF acid solution, 60 min, with ultrasonic cleaner assisting. It can be seen from the curve in Fig. 5 that the AR of the grooves increases with the increase of the laser average power. Some examples include: when the laser average power is 5.0 mW, the AR is 15.5, with the depth of 63.2 μm and the width of 4.1 μm; when the laser average power is 15.0 mW, the AR is 28, with the depth of 118.4 μm and the width of 4.2 μm; when the laser average power is 40.0 mW, the AR is 44, with the depth of 286 μm and the width of 6.5 μm. Meanwhile, the entrance width of the silicon grooves increases with the increase of the laser average power, which can be seen from the insets in Fig. 5.

Silicon is opaque material; the laser wavelength 800 nm in our experiments is located at the absorption region of silicon. When the incident laser average power increases, more laser energy would be absorbed by the silicon materials, this leads to the increase of the RIC microstructures depth. Meanwhile, as the effective spot size of the laser beam increases with the increase of the laser average power, the effective irradiation areas on the silicon surface increases; therefore, the width and the entrance width of the RIC microstructures and the chemical etching induced grooves increase respectively. Furthermore, because the density of the femtosecond laser induced dangling bonds increases with the laser average power increasing [23,24], more foreign O species would be trapped into the interior of silicon; this would accelerate the chemical etching rate. Therefore, due to the increase of the depth and the slight increase of the width of the silicon grooves, the AR increases with the increase of the laser average power.

3.2.3. AR versus υ

Fig. 6 illustrates the dependence curve of the AR of the silicon grooves on the laser scanning velocities, and the insets show the morphology of the grooves accordingly. The laser irradiation parameters are: NA = 0.30 (10×), $P = 30.0$ mW, $\Delta d = 80$ μm. The chemical etching conditions are: 20 wt% HF acid solution, 60 min, with ultrasonic cleaner assisting. It can be seen from the curve in Fig. 6 that the AR of the grooves decreases with the increase

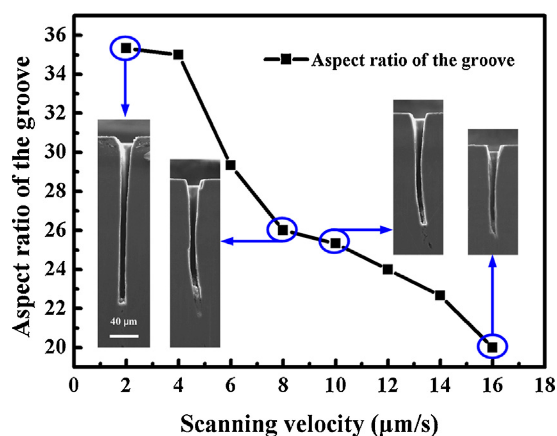

Fig. 6. Dependence curve of AR on the laser scanning velocity (υ). The scale in the inset is 40 μm. (For interpretation of the references to color in figure legend, the reader is referred to the web version of the article.)

of the laser scanning velocity. Some examples include: when the laser scanning velocity is 2 μm/s, the AR is 35.3, with the depth of 216.4 μm and the width of 6.2 μm; when the laser scanning velocity is 8 μm/s, the AR is 26, with the depth of 156.1 μm and the width of 6.2 μm; when the laser scanning velocity is 16 μm/s, the AR is 20, with the depth of 122.4 μm and the width of 6.2 μm. According to these results, we can see that the depth of the grooves decreases with the laser scanning velocity increasing. This is because the laser energy accumulated on unit area of the silicon samples decreases while the scanning velocity increases. Meanwhile, when the laser scanning velocity increases, there is no significant variations of the entrance width of the grooves; this could be attributed to the dependency of the effective irradiation area on the incident laser average power. Therefore, the decrease of the AR of silicon grooves is due to the decrease of the groove depth and the invariation of the groove caused by the increase in laser scanning velocity.

3.3. Summations and further works

According to the analysis of the dependencies of the AR of the silicon grooves on the femtosecond laser irradiation parameters, we could conclude as following: Firstly, the NA of the microscope objective lens mainly influences the cross-sectional shape of the grooves; in order to fabricate silicon grooves with single slim shape, microscope objective lens with low NA should be employed. Secondly, the incident laser average power mainly influences the entrance width and depth of the silicon grooves, in order to produce deep silicon grooves with wide entrance, high incident laser average power is necessary. Finally, the laser scanning velocity mainly influences the depth of the grooves, in order to produce deep silicon grooves, low scanning velocity is needed in the irradiation process, however, it is at the expense of the low productiveness. In summation, in order to fabricate HAR silicon grooves, the laser irradiation parameters mentioned above should be synthetically considered.

Even so, there still are some further works to improve the quality of the silicon grooves and the etching rate of the laser irradiated silicon in this method. Firstly, since the content of the incorporated O species in the RIC microstructures decreases with the increase of the depth, the tails of the RIC microstructures have not been completely eliminated after HF acid solution etching, as shown in Fig. 3(e). We are seeking some post processes to remove these tails. For example, annealing the silicon wafers with grooves in ambient air and then re-etching them with strong acid solutions (such as HNO_3-based solutions). Secondly, in our experiments, we only considered the influences of the irradiation parameters on the silicon grooves, in fact, the chemical etching conditions, such as the HF acid solution concentration, the etching time and the environment temperature also influence the groove quality and the etching rate, and the related works are in progress. Thirdly, according to the formation mechanism of the grooves, the cross-sectional shapes of the grooves are mainly determined by those of the RIC microstructures; therefore, the cross-sectional shapes of the grooves could be controlled via the laser beam shaping technology. Finally, under the same chemical selective etching conditions, the removing level of the RIC microstructures mainly determined by the content of foreign O species incorporated; therefore, if the femtosecond laser irradiation is conducted in ambient oxygen or oxygen-rich gas, there will be more O species incorporated into the photoinduced RIC microstructures, and then the etching rate and the AR of the silicon grooves will be further improved.

4. Conclusions

In conclusion, a simple and practical method for the HAR all-silicon grooves has been proposed. In this method, via the combination of the 800-nm femtosecond laser irradiation with the chemical selective etching, RIC microstructures and all-silicon grooves with the maximum AR of 44, depth of 286 μm and width of 6.5 μm were successfully produced in p-type single crystal silicon wafers. The formation mechanism of the silicon grooves was attributed to the chemical reaction of HF acid solution with the laser induced SiO_2 in the RIC microstructures. The dependence of the AR of the silicon grooves on the laser irradiation parameters, such as: the numerical apertures (NA) of the microscope objective lens, the laser average powers (P), the laser scanning velocities (υ), were systematically discussed. Due to its low cost, high selectivity, high etching rate, high flexibility, and high potential impact-on, we predict that this method would be a promising method for the fabrication of silicon-based advanced functional materials and MEMS devices.

Acknowledgements

The authors gratefully acknowledge the financial support for this work provided by the National Natural Science Foundation of China (NSFC) under the Grant nos. 91123028 and 61235003, and the National Basic Research Program of China (973 Program) under Grant no. 2012CB921804. The authors also sincerely thank Ms. Dai at International Center for Dielectric Research (ICDR) in Xi'an Jiaotong University for the support of SEM and EDS measurements.

References

[1] S. Ogawa, S. Soda, S. Lee, S. Izuo, Y. Yoshida, Sensors and Actuators A 181 (2012) 77–80.
[2] X. Wang, W. Zeng, G. Lu, O.L. Russo, E. Eisenbraun, Journal of Vacuum Science and Technology B 25 (2007) 1376.
[3] D.S. Engstrom, Y. Soh, Journal of Vacuum Science and Technology B 31 (2013) 021806.
[4] T. Ito, K. Karahashi, S. Kang, S. Hamaguchi, Journal of Vacuum Science and Technology A 31 (2013) 031301.
[5] S. Surdo, S. Merlo, F. Carpignano, L.M. Strambini, C. Trono, A. Giannetti, F. Baldini, G. Barillaro, Lab on a Chip 12 (2012) 4403–4415.
[6] G. Barillaro, L.M. Strambini, V. Annovazzi-Lodi, S. Merlo, IEEE Journal of Selected Topics in Quantum Electronics 15 (2009) 5.
[7] E.V. Astrova, V.A. Tolmachev, G.V. Fedulova, V.A. Melnikov, A.V. Ankudinov, T.S. Perova, Applied Physics A 98 (2010) 571–581.
[8] E. Hendry, F.J. Garcia-Vidal, L. Martin-Moreno, J.G. Rivas, M. Bonn, A.P. Hibbins, M.J. Lockyear, Physical Review Letters 100 (2008) 123901.
[9] K.F. Jensen, Materials Research Society Bulletin 31 (2006) 101–107.
[10] L. Sainiemi, T. Nissil, V. Jokinen, T. Sikanen, T. Kotiaho, R. Kostiainen, R.A. Ketola, S. Franssila, Sensors and Actuators B 132 (2008) 380–387.
[11] S. Tachi, K. Tsujimoto, S. Okudaira, Applied Physics Letters 52 (1988) 616.
[12] R. St-Gelais, J. Masson, Y. Peter, Applied Physics Letters 94 (2009) 243905.
[13] K.W. Kok, W.J. Yoo, K. Sooriakumar, Journal of Vacuum Science and Technology B 20 (2002) 154.

[14] C. Strandman, L. Rosengren, H.G.A. Elderstig, Y. Backlund, Journal of Microelectronic Systems 4 (1995) 4.
[15] V.A. Tolmachev, E.V. Astrova, J.A. Pilyugina, T.S. Perova, R.A. Moore, J.K. Vij, Optical Materials 27 (2005) 831–835.
[16] G. Canavese, S.L. Marasso, M. Quaglio, M. Cocuzza, C. Ricciardi, C.F. Pirri, Journal of Micromechanics and Microengineering 17 (2007) 1387–1393.
[17] M. Bengtsson, S. Ekstrom, G. Marko-Varga, T. Laurell, Talanta 56 (2002) 341–353.
[18] G.V. Treyz, R. Beach, R.M. Osgood, Applied Physics Letters 50 (1987) 8.
[19] G.V. Treyz, R. Beach, R.M. Osgood, Journal of Vacuum Science and Technology B 6 (1988) 1.
[20] M. Mullenborn, H. Dirac, J.W. Petersen, Applied Physics Letters 66 (1995) 22.
[21] T.H.R. Crawford, A. Borowiec, H.K. Haugen, Applied Physics A 80 (2005) 1717–1724.
[22] K. Venkatakrishnan, N. Sudani, B. Tan, Journal of Micromechanics and Microengineering 18 (2008) 075032.
[23] T. Kudrius, G. Slekys, S. Juodkazis, Journal of Physics D: Applied Physics 43 (2010) 145501.
[24] Y. Ma, H. Ren, J. Si, X. Sun, H. Shi, T. Chen, F. Chen, X. Hou, Applied Surface Science 261 (2012) 722–726.
[25] A. Somashekhar, S. O'Brien, Journal of the Electrochemical Society 143 (1996) 9.
[26] A.A. Pande, D.S.L. Mui, D.W. Hess, IEEE Transactions on Semiconductor Manufacturing 24 (2011) 1.
[27] B. Tan, Journal of Micromechanics and Microengineering 16 (2006) 109–112.
[28] Z. Sanaee, M. Poudineh, M. Abdolahad, S. Mohajerzadeh, Journal of Micromechanics and Microengineering 21 (2011) 125012.
[29] S. Azimi, A. Sandoughsaz, B. Amirsolaimani, J. Naghsh-Nilchi, S. Mohajerzadeh, Journal of Micromechanics and Microengineering 21 (2011) 074005.
[30] A. Sandoughsaz, S. Azimi, H. Mazreati, S. Mohajerzadeh, Journal of Micromechanics and Microengineering 23 (2013) 035022.
[31] B. Wu, A. Kumar, S. Pamarthy, Journal of Applied Physics 108 (2010) 051101.
[32] H.K. Taylor, H. Sun, T.F. Hill, A. Farahanchi, D.S. Boning, Journal of the Electrochemical Society 153 (2006) 8.
[33] K. Khare, S. Herminghaus, J. Baret, B.M. Law, M. Brinkmann, R. Seemann, Langmuir 23 (2007) 12997–13006.
[34] H. Zhao, K. Law, Langmuir 28 (2012) 11812–11818.
[35] M. Bassu, S. Surdo, L.M. Strambini, G. Barillaro, Advanced Functional Materials 22 (2012) 1222–1228.
[36] G. Barillaro, S. Merlo, S. Surdo, L.M. Strambini, F. Carpignano, Microfluidics and Nanofluidics 12 (2012) 545–552.
[37] J.X. Gao, L.P. Yeo, M.B. Chan-Park, J.M. Miao, Y.H. Yan, J.B. Sun, Y.C. Lam, C.Y. Yue, Journal of Microelectronic Systems 15 (2006) 1.
[38] L.P. Yeo, Y.H. Yan, Y.C. Lam, M.B. Chan-Park, Langmuir 22 (2006) 10196–10203.
[39] Y.R. Shen, The Principles of Nonlinear Optics, Wiley, New York, 1998.